



Radial ballistic-diffusive heat conduction in nanoscale

Han-Ling Li and Bing-Yang Cao

Key Laboratory for Thermal Science and Power Engineering of Ministry of Education, Department of Engineering Mechanics, Tsinghua University, Beijing China

ABSTRACT

Heat conduction in radius direction is of great importance to the use of two-dimensional materials and experiments. In this paper, radial ballistic-diffusive heat conduction in nanoscale is investigated by the phonon Monte Carlo (MC) method and phonon Boltzmann transport equation. We find that owing to the two-dimensional nature, the radial heat transport is dominated by two parameters, including the Knudsen number (Kn) and the radius ratio of the two concentric boundaries, the former of which is defined as the ratio of the phonon mean-free-path to the distance of the two boundaries. Compared with the one-dimensional cases, radial ballistic transport not only leads to boundary temperature jumps and the size effect of the effective thermal conductivity, but also results in a nonlinear temperature profile in logarithm radius coordinate, a difference of the inner and outer boundary temperature jumps, a stronger size effect, and a nonuniform local thermal conductivity within the system. When the value of Kn is far less than one, diffusive transport predominates and the effect of the radius ratio is negligible. Whereas, when Kn is comparable to or larger than one, the intensity of ballistic transport compared to diffusive transport will be increased significantly as the radius ratio decreases. In addition, the models for the temperature profile and the effective thermal conductivity are derived by an interpolation of the limit solutions and modification of the previous model, respectively. The good agreements with the phonon MC simulations demonstrate their validity.

ARTICLE HISTORY



Received 20 June 2018
Revised 22 August 2018
Accepted 1 September 2018

KEYWORDS

Nanoscale; radial heat conduction;
ballistic-diffusive transport;
phonon Monte Carlo

Introduction

The breakdown of Fourier's law at nanometer to micrometer scales has important implications for nanoelectronics and has received a great deal of recent attention [1–3]. Although previous studies mainly focused on one-dimensional (1D) non-Fourier heat conduction in nanowires [4], nanofilms [5, 6], and superlattices [7], the extensive two-dimensional (2D) thermal transports existing in recent applications establish radial heat conduction as a worth investigating process. The radial heat conduction means heat is conducted along the radius direction [8], which usually occurs in flat systems heated by a point source, such as silicon nanofilms in transistors [9] and graphene sheets [10] in small electronic devices. It also plays an important role in encapsulated nanowires [11], where the heat generated in the inner material needs to be dissipated to the outer ambience. Besides, advanced time-domain thermoreflectance (TDTR) and frequency-domain thermoreflectance (FDTR) techniques both require reliable models accounting for the radial heat transport to extract the desired thermal properties [12]. In a word, better understanding of the nanoscale radial heat conduction is beneficial to the applications of 2D structures and experimental measurements.

CONTACT Bing-Yang Cao  caoby@tsinghua.edu.cn  Department of Engineering Mechanics, Key Laboratory for Thermal Science and Power Engineering of Ministry of Education, School of Aerospace Engineering, Tsinghua University, Beijing 100084, P. R. China
Color versions of one or more of the figures in the article can be found online at www.tandfonline.com/umte.

When the characteristic length (L) of a nanoscale system is comparable to the phonon mean-free-path (MFP), the phonon-boundary scattering and the ballistic transport give rise to the experimentally observed failure of Fourier's law [13–16]. The Knudsen number, which is defined as $Kn = l_0/L$ (l_0 denotes the value of MFP in bulk materials), has a decisive role on phonon transport. Fourier's law is only valid for the diffusive limit ($Kn \rightarrow 0$), and the ballistic limit at $Kn \rightarrow \infty$ is also known as the Casimir limit [17]. Chen [5] adopted the ballistic-diffusive equations derived from phonon Boltzmann transport equation (BTE) to study the 1D non-Fourier heat conduction across thin films. Li [18] pointed out that the thermal conductivity in 1D systems could be expressed in terms of the system size as $k = cL^\beta$, where the ballistic-diffusive regime corresponds $0 < \beta < 1$. The reduction of the thermal conductivity in 1D systems could also be predicted in theory by extended irreversible thermodynamics [19], phonon hydrodynamics [20] and Landauer approach [21]. Moreover, for heat conduction generated by imposing boundary temperature, a remarkable physical feature is boundary temperature jump (δT) [22], which refers to the mismatch between the temperature of the heat sink and temperature just inside the system. Consequently, the input temperature difference can be expressed as $\Delta T = \int dx \nabla T + \delta T_1 + \delta T_2$ (the subscript refers to different boundaries). It has been observed that the temperature gradient inside 1D systems is a constant [22, 23], and theoretical models to predict the jump values have been proposed by different approaches. Hua and Cao [24] used the acoustically thin approximation for $Kn \gg 1$ and the diffusive approximation for $Kn \ll 1$ to solve phonon BTE, then they averaged the two limit solutions for the middle Knudsen numbers. Maassen and Lundstrom [25] adopted the McKelvey-Shockley flux method, and Sobolev [26] used the discrete variables formalism. These models are all in good agreements with the results of molecular dynamics (MD) and phonon MC simulations.

In multi-dimensional heat conduction where the heat is transported in multiple directions, the non-Fourier heat conduction has been found to be dependent on more factors, owing to the complex configurations of the system. Lepri et al. [27] suggested that the thermal conductivity of 2D anharmonic crystals diverge with the system size as $k \sim \ln(L)$. Chen et al. [28] found that the surface-to-volume ratio could have a significant influence on the thermal conductivity of silicon nanowires. Based on BTE, Hua and Cao [29] established analytical models accounting for the longitudinal and lateral constraints in nanostructures to predict the effective thermal conductivity, and the similar method was applied to 2D periodic nanoporous films, too [30]. Due to the complexity of the analysis and excessive computational cost of the numerical simulation for a general multi-dimensional heat transport, the axisymmetric radial heat conduction is deemed to be a simple but effective way to study the characteristics of the non-one-dimensional heat conduction in nanoscale. Based on phonon hydrodynamics and thermomass theory, Sellitto et al. [31, 32] found that the temperature could rise along the radius direction when the distance to the point heat source was less than l_0 . By utilizing MD simulation, Yang et al. [33] predicted the graded thermal conductivities in nanoscale graphene disks whose outer radii were smaller than the value of MFP. Wilson and Cahill [34] emphasized that the radius of the pump light (heat source) could have a decisive effect on the results of TDTR and FDTR. These reported studies all stated that the relation between the radius and the MFP affected radial phonon transport, however, systematic and in-depth understanding and modeling of the nanoscale radial heat conduction is still lacking.

In the present work, we use the phonon tracing Monte Carlo (MC) method and theoretical analyses based on phonon BTE to study the steady-state radial ballistic-diffusive heat conduction in nanoscale. Radial phonon transport is found to be determined by two individual parameters, one is the Knudsen number calculated by using the difference between the outer and inner radius as the characteristic length, and the other is the radius ratio of the concentric boundaries (r_{12}). Radial ballistic transport will cause the temperature distribution to change non-linearly with the logarithm radius coordinate, the temperature jumps at the two boundaries to be different, the size effect of the effective thermal conductivity to be stronger and the local thermal conductivity within the system to

be nonuniform. More importantly, the phonon-boundary scattering and the ballistic effect increases remarkably as r_{12} decreases, except for the cases of $Kn \ll 1$. In addition, theoretical models for the temperature profile and effective thermal conductivity have been proposed, which compare favorably with the results of phonon MC simulations. These simulations and models could be helpful for predicting thermal transport in 2D nanoscale devices and experiments.

Methods

The schematic diagram of radial heat conduction is illustrated in Figure 1 (a), in which two isothermal heat sinks with a hot and cold temperature (T_h and T_c) are set at the inner (subscript 1) and the outer (subscript 2) boundary, respectively, to produce heat flow along the radius direction. The corresponding cylindrical coordinate systems are schematically shown in Figure 1 (b), in which the subscript “c” represents the parameters related to the fixed coordinate system. Thermal properties only vary with the radius direction r , but not with the axial position z or azimuthal angle ψ_c in radial heat conduction.

The phonon BTE under relaxation time approximation in steady state is

$$\mathbf{v}_g \cdot \nabla f = \frac{f_0 - f}{\tau} \quad (1)$$

where \mathbf{v}_g , f , f_0 , and τ denotes the group velocity vector, phonon distribution function, the Bose-Einstein distribution in equilibrium and the relaxation time, respectively. Assuming the group velocity is isotropic and does not vary with the location, we have $\mathbf{v}_g = v_g \mathbf{s}$ where \mathbf{s} is a unit direction vector. By introducing linear dimensionless radial coordinate as $r^* = r/v_g \tau$, Eq. (1) is transformed to

$$\sin \theta \cos \psi \frac{\partial f}{\partial r^*} - \sin \theta \sin \psi \frac{1}{r^*} \frac{\partial f}{\partial \psi} = f_0 - f \quad (2)$$

Compared to BTE in 1D systems as $\cos \theta_x \frac{df}{dx} = f_0 - f$ (θ_x denotes the angle with the x axis), there is a term about the derivate of angle ψ in Eq. (2), which is mathematically originated from $d\psi_c + d\psi = 0$ along the \mathbf{s} direction as Figure 1 (b) illustrates. Similar result has been discussed in the gray media radiation [35] and it is not contradictory to the fact that the heat is conducted along the radius direction. In fact, the additional term introduces more intriguing characteristics of phonon transport, but it also perplexes the analytical solution of Eq. (2).

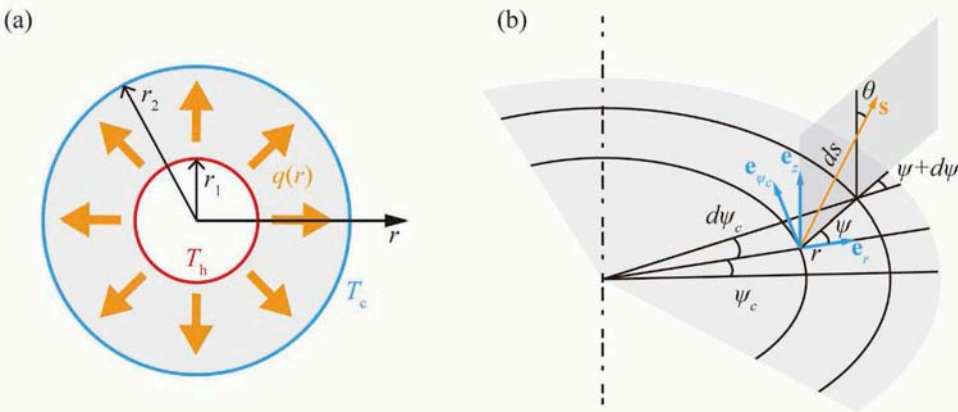


Figure 1. (a) The schematic diagram of radial heat conduction; (b) the cylindrical coordinate systems.

Eq. (1) is mostly solved by numerical approaches, among which phonon tracing MC, which is especially flexible with use for complex geometric structures and readily include different scattering events, has been extensively developed [24, 29, 30, 36, 37]. So it is employed in this paper. We focus on the effect of phonon-boundary scattering and ignore the scattering of imperfections and impurities. The Debye theory and gray-body approximation are employed to simplify the problem, and the temperature difference between the two heat sinks is set to be small enough compared with their absolute values. Since Eq. (1) is a linear equation, the simulated system is reduced to $T_1 = T_h - T_c$ and $T_2 = 0$, which significantly reduces the simulation time without any penalty on the accuracy. To ensure the convergence of the results and reduce random errors, all phonon MC simulations are performed with the total number of phonon bundles at least being $N = 2 \times 10^6$. More details of the phonon tracing MC method can be found in Ref. [24].

The thermal conductivity in non-metallic crystalline materials actually results from cumulative contributions of phonons that have a broad range of MFPs and frequency [38], making phonon dispersion be an important factor affecting heat transport [39, 40]. When considering the actual phonon dispersion, phonon transport must be described by MFP spectra, which can be achieved by redetermining the MFP of each phonon bundle after phonon-phonon scattering in the steady-state MC simulation [41]. For the analysis of BTE, there two efficient approaches to take the phonon dispersion into consideration: (a) calculating the boundary confined MFP for each phonon mode and integrating over the frequency [42, 43]; (b) using the phonon MFP spectra function [44]. Introducing complex phonon dispersion could get more accurate and comprehensive results, but it is bound to increase the computational costs and the complexity of theoretical models, which make it difficult to distinguish different factors that affect thermal transport. To simplify, gray-body approximation with a proper and representative MFP has been extensively utilized in the studies of phonon-boundary scattering [14, 16, 23, 45] and ballistic transport [19, 29, 46, 47]. Ignoring some sacrifice on the accuracy, the good agreements between the predicted results and experimental measurements have established the use of a proper and representative MFP as an effective simplification [14, 16, 19, 23, 29, 45, 46]. In this paper, since our major concern is how to describe the influence of the cylindrical geometry on phonon ballistic-diffusive heat conduction efficiently, gray-body approximation with a representative MFP is adopted to validate our analyses of the impact of the geometric parameters and the developed prediction models.

Results and discussions

The geometric configuration of the system in radial heat conduction can be determined by two individual parameters, as the inner and outer radius of the boundaries shown in Figure 1 (a). However, direct use of the radii is not conducive to study the possible effect of the size and shape on heat transport, therefore another set of parameters is chosen in our work. On the one hand, as an analogy to 1D ballistic-diffusive heat conduction, the distance between the two heat sinks is defined as the characteristic length ($L = r_2 - r_1$). On the other hand, the radius ratio ($r_{12} = r_1/r_2$), which reflects the geometric discrepancy between the radial heat conduction and the 1D heat conduction in films, works as the shape parameter. In the limit of $r_{12} \rightarrow 1$, the radial heat conduction reduces to 1D case. Such description of the geometric configuration was also adopted in photon radiation between concentric cylinders [48]. In this way, the corresponding Knudsen number defined as $Kn = l_0/(r_2 - r_1)$ is expected to have the similar effect on phonon transport as in 1D heat conduction, and new-found phenomena in radial heat conduction can be attributed to the effect of r_{12} , which will be discussed in the following parts.

Temperature profiles

We begin by calculating the temperature profiles along the radius direction with different Kn and r_{12} , as illustrated in Figure 2. According to Fourier's law and the energy conservation in steady state, the governing equation of the temperature is

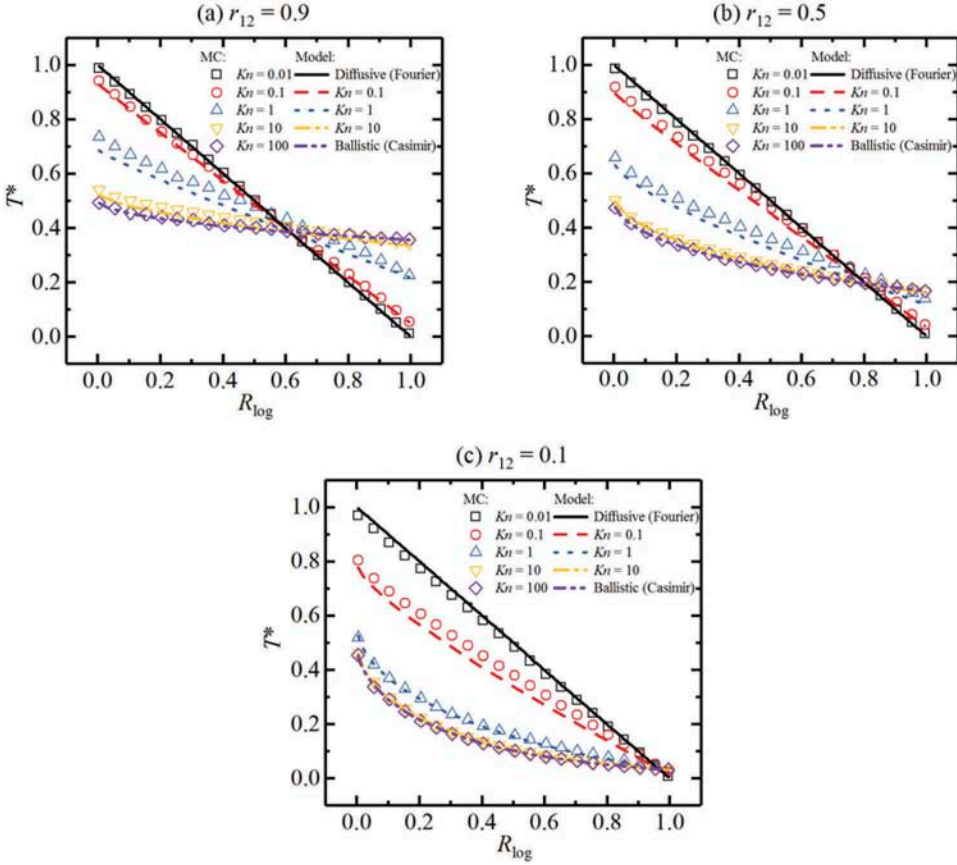


Figure 2. Temperature profiles along the radius direction. The theoretical solutions are calculated by Eq. (8). “Diffusive” refers to the diffusive limit, and “Ballistic” refers to the ballistic limit.

$$-2\pi r \cdot k_b \frac{\partial T}{\partial r} = Q \quad (3)$$

where k_b is the thermal conductivity in bulk materials, Q is the heat flow (with a unit length in z axis) along the radius direction. Ignoring the change of k_b with temperature, we have

$$\frac{\partial T}{\partial \ln r} = -\frac{Q}{2\pi k_b} = \text{const} \quad (4)$$

which indicates that temperature varies linearly with the logarithmic coordinate. For simplicity and clarity, normalized dimensionless coordinates as $T^* = \frac{T-T_c}{T_h-T_c}$ and $R_{\log} = \frac{\ln(r/r_1)}{\ln(r_2/r_1)}$ are adopted, and the result of Fourier’s law is (subscript “D” refers to “diffusive limit”)

$$T_D^* = 1 - R_{\log} \quad (5)$$

By using the logarithmic radius coordinate, the influence of the varied cross-sectional area along the heat flow direction on temperature distribution can be eliminated in Fourier’s law, so the oblique solid lines depicted in Figure 2 are the same for different r_{12} . When $Kn = 0.01$, the system size is so large that Fourier’s law is a good approximation and the change of r_{12} nearly doesn’t affect the

temperature profiles. For $Kn = 0.1$, Fourier's law loses its accuracy and temperature jumps occur at the two boundaries. As Kn increases, the boundary temperature jumps become more significant, and the temperature gradually varies with R_{\log} in a non-linear way, as the results of $Kn = 10$ show. When it comes to $Kn = 100$, the system size is so small that almost all phonons are transported in ballistic ways, making the temperature profiles be quite close to the Casimir limit, which with reference to the photon radiation [48] can be written as (subscript "B" refers to "ballistic limit")

$$T_B^* = \frac{1}{\pi} \arcsin\left(r_{12}^{R_{\log}}\right) \quad (6)$$

In contrast to Eq. (5), temperature profile predicted by Eq. (6) will change with r_{12} even in the logarithm radius coordinate. Comparing Figure 2 (a) ~ (c), although the temperature profile's dependence on Kn is the same with that in 1D systems as expected, the value of r_{12} is found to have a remarkable influence on the temperature profiles. The deviation from Fourier's law is more notable for a smaller r_{12} . Take $Kn = 0.1$ as an example, the dimensionless value of the inner boundary temperature jump is less than 0.05 at $r_{12} = 0.9$, while it increases to about 0.2 at $r_{12} = 0.1$. Besides, the non-linear change of the temperature is becoming more obvious as r_{12} decreases. The temperature profile still looks like a straight line at $Kn = 1$ and $r_{12} = 0.9$, but the profile of $Kn = 1$ and $r_{12} = 0.1$ has visibly become a curved line, which is also closer to the prediction of Eq. (6). It is concluded that a reduced r_{12} strengthens the ballistic transport, thus the temperature profile for the same Kn is closer to the non-linear results of the Casimir limit.

Theoretical model to predict the temperature profiles are developed, which is also able to quantitatively describe the intensity of the ballistic effect. In a thermal non-equilibrium state, temperature is usually defined as a representation of the average energy of all phonons around a local point [7]. Since ballistic-diffusive transport can be interpreted as the concurrence of diffusive and ballistic phonons, the results of Fourier's law and Casimir limit can be termed as two bounds for the local phonon energy (denoted as $E(r)$) at $Kn \rightarrow 0$ and $Kn \rightarrow \infty$. For example, the boundary temperature jumps demonstrated in Figure 2 are always between 0 (totally diffusive) and the values of the Casimir limit (totally ballistic). For a middle Kn , $E(r)$ can be calculated by an interpolation of the two bounds as

$$E(r) = \eta E_B(r) + (1 - \eta) E_D(r) \quad (7)$$

where η and $1 - \eta$ are the interpolated coefficients for ballistic transport and diffusive transport, respectively. The value of η could be dependent on the system size and shape. The similar interpolation method was used in Hua and Cao's [24] model for predicting boundary temperature jumps. Under the condition of $T_h - T_c \ll T_h \approx T_c$, the temperature within the system is linearly dependent on the local energy, thus it can be calculated as

$$T(r) = \eta T_B(r) + (1 - \eta) T_D(r) \quad (8)$$

The only unknown in Eq. (8) is the coefficient η , which can be calculated by the temperature jump model to be given in Sec. 3.2. The results predicted by Eq. (8) for the middle three Knudsen numbers are also plotted Figure 2, which agree well with those by phonon MC simulations. It should be noted that Eq. (8) is not always satisfied within the system, and the simulated temperature at some points could be higher than the two bounds, such as $R_{\log} = 0.6$ at $Kn = 1$ shown in Figure 2 (a). However, since the deviations of the model and phonon MC simulation at these points are less than 5%, Eq. (8) is concluded to be a good and simple estimation. The values of η for different Kn and r_{12} are shown in Table 1, where η always increases with Kn for a fixed r_{12} as expected. More importantly, when Kn is fixed, η also increases dramatically with r_{12} decreasing. For $Kn = 1$, η is about 40% larger for $r_{12} = 0.1$ (0.877) than $r_{12} = 0.9$ (0.612). Because the value of η in some extend represents the intensity of

Table 1. The calculated values of η based on Eq. (10).

Kn	$r_{12} = 0.9$	$r_{12} = 0.5$	$r_{12} = 0.1$
0.01	0.016	0.024	0.064
0.1	0.137	0.194	0.403
1	0.612	0.702	0.877
10	0.940	0.956	0.985
100	0.994	0.996	0.999

ballistic transport compared to diffusive transport, Table 1 distinctly demonstrates that besides increasing Kn , decreasing r_{12} will also strengthen the ballistic transport in radial heat conduction.

Boundary temperature jumps

As mentioned in Sec. 1, the boundary temperature jump is an important feature of the phonon-boundary interactions in ballistic-diffusive regime, and knowing the value of temperature jump is also essential to describe the temperature profile. The phonon MC simulated results of the inner and outer boundary temperature jumps are shown in Figure 3 (a) and (b), where the results of 1D systems are drawn for comparison. When r_{12} is fixed, the dependence of the temperature jump varying with Kn has the similar trend with 1D case. For $Kn = 0.01$, the temperature jumps are very close to the diffusive limit, while the results of $Kn = 100$ almost equal to the ballistic limit. For the middle Knudsen numbers, the jump values are between the Casimir limit and Fourier's law, proving that they can be used as the two bounds of phonon transport again. Moreover, the temperature jump values at the inner boundary are always greater than the results of the same Kn in 1D systems, while at the outer boundary less than those in 1D systems, and the deviations are getting more significant as Kn increases or r_{12} decreases. This is caused by the reduction of the value of temperature gradient along the heat flow direction in radial heat conduction. The value of boundary temperature jumps can be expressed as $\delta T_i = \gamma |\nabla T|_i$, where $\nabla T|_i$ is the internal temperature gradient extrapolated to the boundary i [22]. The change of the proportionality coefficient γ can be ignored for the tiny temperature difference and the same type boundary thermostats, thus the absolute value of $\nabla T|_i$ predominates the boundary temperature jump. The temperature gradient inside 1D systems is a constant owing to the symmetric configuration, so that the boundary temperature jumps are the same. In radial heat conduction, $|\nabla T| = \frac{1}{r} \left| \frac{dT}{d \ln r} \right|$ will decrease with r even calculated by Fourier's law. Besides, the ballistic transport will also increase the degree of change in temperature gradient by the changing the value of

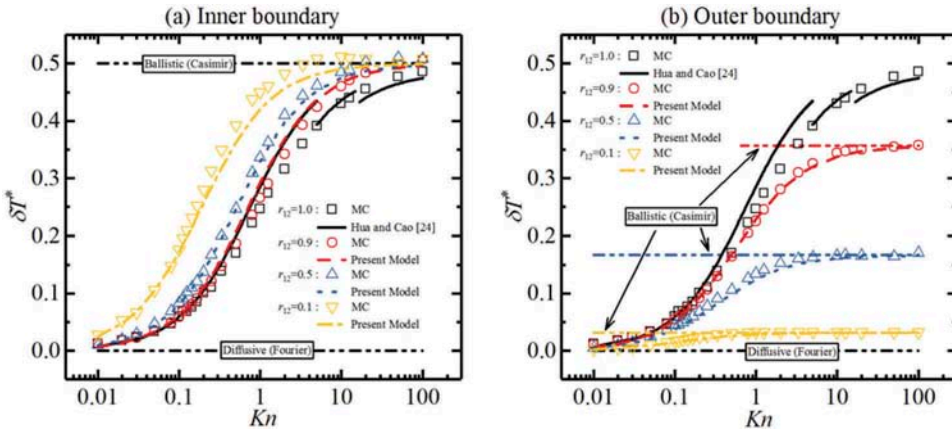


Figure 3. The boundary temperature jumps varying with Kn at different r_{12} : (a) the inner boundary and (b) the outer one. The results of 1D systems are shown as “ $r_{12} = 1.0$.”

$|dT/d\ln r|$ as shown in Figure 2. The two factors contribute to the higher and lower temperature jumps than those in 1D systems at the inner and outer boundary. More importantly, with r_{12} decreasing, since the greater deviations cannot be explained by only considering the change of boundary radii, a stronger ballistic transport is supposed to exist.

To better study the effect of r_{12} on the boundary temperature jumps, the ratios of the outer and inner jumps are illustrated in Figure 4. For 1D systems, the ratio is always one and does not change with Kn , as the solid line shows. For radial heat conduction, when $Kn \rightarrow \infty$, Eq. (6) gives the Casimir limit value of the ratio as $2 \arcsin(r_{12})/\pi$. Considering that there is no boundary temperature jump in the limit of $Kn \rightarrow 0$, the result under the condition of $Kn \ll 1$ is adopted as another meaningful boundary condition to calculate the ratio of boundary temperature jump, instead of Fourier's law. Since the characteristic length is sufficiently large in this case, most phonons are in diffusive regime and the diffusive approximation can be used. With reference to the diffusion solution proposed for radiation transfer equation [49], we derive $\frac{dT}{d\ln r} = \text{const}$ within the system, which has been confirmed by the simulated temperature profiles at $Kn = 0.01$ in Figure 2, and the temperature jump ratio can be calculated as $\delta T_2/\delta T_1 = r_2/r_1 = r_{12}$. It can be seen from Figure 4 that the ratios of the middle Knudsen numbers are certainly varying between the predictions of the diffusive approximation and the Casimir limit. Besides, the location where the boundary temperature jump ratio starts to deviate from the prediction of the diffusive approximation comes earlier with r_{12} decreasing, verifying that a small r_{12} enhances the ballistic transport. It is worth noting that a stronger ballistic transport could lead to a smaller boundary temperature jump, as shown in Figure 3 (b), which is attributed to the lower value of temperature gradient adjacent to the outer boundary.

Similarly, a theoretical model to predict the boundary temperature jump can be established by the interpolation between the solutions at $Kn \ll 1$ and $Kn \rightarrow \infty$, as we did for the temperature profile. When $Kn \ll 1$, since r_{12} has little effect, the derivative of the angle ψ in Eq. (2) can be ignored, and the problem reduces to the 1D case, where the boundary temperature jump could be calculated as $\delta T^* = \frac{1}{2} q^*$ by solving phonon BTE under the diffusive approximation [24]. The dimensionless heat flux is defined as $q^* = \frac{q}{\sigma_p(T_h^4 - T_c^4)}$, in which σ_p denotes the phonon Stephen-Boltzmann constant. By using the effective thermal conductivity to be calculated in Sec. 3.3, the temperature jump can be calculated as (take the inner boundary as an example):

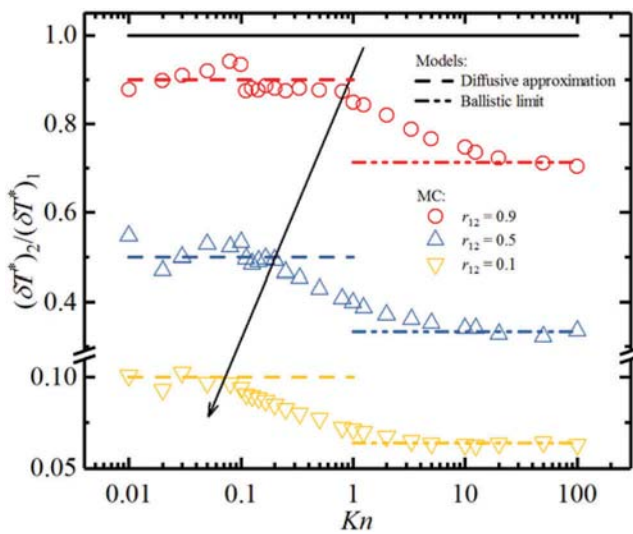


Figure 4. The ratios of boundary temperature jumps varying with Kn . The horizontal solid line refers to the 1D case. The dash and dash-dotted-dotted lines are the predictions of diffusive approximation and ballistic limit, respectively.

$$(\delta T^*)_{1,DA} = \frac{2(1-r_{12})}{3r_{12} \ln(1/r_{12})} \frac{1}{(\alpha + 1/Kn)} \quad (9)$$

where the subscript “DA” refers to the diffusive approximation and α is a parameter only dependent on r_{12} . Eq. (9) approaches to zero as $Kn \rightarrow 0$, which is consistent with Fourier’s law. Besides, it will result in a nonzero constant if we directly let $Kn \rightarrow \infty$. Although the value of the constant is bound to deviate from the correct value predicted by Eq. (6), the function form of Eq. (9) is worthy of reference. Thus, we have an empirical expression of the boundary temperature jumps for the middle Knudsen numbers as

$$\delta T^* = \frac{1}{a + b/Kn} \quad (10)$$

The values of a and b , which are different for the inner and outer boundary, are determined by the results of the diffusive approximation at $Kn \ll 1$ (we actually choose $Kn = 0.01$ in calculations) and the Casimir limit at $Kn \rightarrow \infty$. Thus, we have $a_i = \frac{1}{(\delta T^*)_{i,B}}$ and $b_i = \frac{1}{100} \left[\frac{1}{(\delta T^*)_{i,DA}} - \frac{1}{(\delta T^*)_{i,B}} \right]$, in which $i = 1$ or 2 refers to the inner or the outer boundary. As $Kn \rightarrow 0$, Eq. (10) automatically agrees with Fourier’s law. The results predicted by Eq. (10) are also depicted in [Figure 2](#), which are in good consistency with phonon MC simulations, with the maximum absolute error being less than 0.04. Taking the random error of phonon MC simulations into consideration, the validity of the present model has been confirmed. In addition, interpolation by Eq. (10) avoids the discontinuities produced by the simple averaging in Hua and Cao’s 1D model. After establishing the boundary temperature jump model, an interpolation between the diffusive and ballistic limit is conducted to get $\eta_i = \left[1 + \frac{1}{100Kn} \left(\frac{(\delta T^*)_{i,B}}{(\delta T^*)_{i,DA}} - 1 \right) \right]^{-1}$. There is a little difference between the value of η calculated at the inner and the outer boundary owing to the approximate model. To get a good accuracy at the both boundaries, arithmetical averaging is adopted to derive the final value of η as $\eta = (\eta_1 + \eta_2)/2$, which gives the results shown in [Table 1](#).

The effective and local thermal conductivities

Besides the boundary temperature jump, the effective thermal conductivity is also employed to characterize the radial ballistic-diffusive heat conduction. Based on Fourier’s law, it is easy to derive the expression of the total heat flow (with a unit length along the z axis) for the diffusive limit as $Q_D = 2\pi k_b (T_h - T_c) / \ln(r_2/r_1)$, in which k_b denotes the thermal conductivity in bulk materials. Using the total heat flow to define the effective thermal conductivity for the radial heat conduction, it can be calculated as

$$k_{\text{eff}} = \frac{\ln(r_2/r_1)}{2\pi} \frac{Q}{T_h - T_c} \quad (11)$$

where Q calculated by phonon MC simulations varies with Kn and r_{12} . [Figure 5](#) shows the simulated effective thermal conductivities varying with the acoustic length ($1/Kn$). The ratios of the effective thermal conductivities to its bulk values are found to reduce with r_{12} decreasing for a fixed Kn , which demonstrates a stronger ballistic transport, though the results of $r_{12} = 1.0$ and $r_{12} = 0.9$ is not easy to distinguish by eye. At $r_{12} = 1.0$, the effective thermal conductivity could be estimated by $k_{\text{eff}} = cL^\beta$, in which the value of β relates to the value of Kn . The results of the piecewise fitting are shown as the solid lines in [Figure 2](#), where the fitted values of β are also exhibited. The decrease of β with the acoustic length means the intensity of ballistic transport compared with diffusive transport is decreasing. For $Kn \leq 0.05$, $\beta \rightarrow 0$ indicates that the thermal conductivity does not change with the system size. For $Kn \geq 10$, the

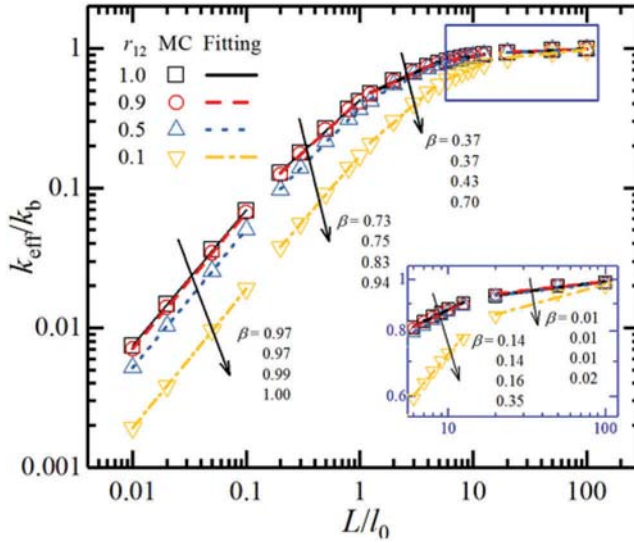


Figure 5. The effective thermal conductivities varying with the acoustic length. The lines are the fitting results by $k_{\text{eff}}=cL^\beta$.

ballistic transport is so strong that k_{eff} nearly increases linearly ($\beta = 0.97$) with the acoustic length. For $r_{12} \neq 1.0$, the simulated results are found to have the similar trends with that of the $r_{12} = 1.0$ case, and we assume that $k_{\text{eff}} \propto L^\beta$ is still valid by regarding radial heat conduction as an 1D transport process in cylinder coordinates. The values of β are larger for a smaller r_{12} in the same segments in [Figure 5](#), quantitatively demonstrating that the intensity of ballistic transport increases once more.

To put the new-found fact that radial ballistic-diffusive transport is dependent on r_{12} into perspective, the interactions between phonons and the boundaries are going to be estimated. [Figure 6](#) depicts the geometric configurations of different r_{12} with the same L , it can be clearly seen that a reduced r_{12} intensifies the boundary constraints on phonon transport. When $Kn \ll 1$, phonons will suffer sufficient phonon-phonon scattering before being absorbed by the boundaries, thus almost all phonons are transported diffusively and the effect of boundary constraints can be ignored, as the results of $Kn = 0.01$ in [Figure 2](#) to [Figure 5](#) show. As L becomes comparable to l_0 , phonon-boundary interaction plays an important role. The reduced r_{12} makes phonons emitted from the inner heat sink be more probable to be absorbed by the outer one without any phonon-phonon scattering, leading to a stronger ballistic transport which is dependent on r_{12} as [Eq. \(6\)](#) demonstrates. [Figure 6](#) also shows that decreasing r_{12} will reduce the size of the inner thermal sink, which will lead to stronger ballistic effect as the reference suggests [50]. In fact, the value of r_{12} not only has some influence on the boundary size when using $r_2 - r_1$ as the other characteristic parameter, but also distinctly reflect the effect of the boundary shape. As an evidence, at the ballistic limit predicted by [Eq. \(6\)](#), even r_1 is fixed, the change of r_{12} will also affect the temperature profile, indicating that the effect of r_{12} cannot be totally attributed to the size of the heat sink. It is concluded that both the size and shape will significantly affect the thermal transport owing to the 2D natural character of the radial heat conduction.

The value of the effective thermal conductivity can also be predicted without any numerical simulation. Under the condition that utilizing temperature difference to produce heat flow, Majumdar [23] proposed a gray model for the 1D effective thermal conductivity as $\frac{k_{\text{eff}}}{k_b} = (1 + \frac{4}{3}Kn)^{-1}$. Referring to the Matthiessen's law, Hua and Cao [51] concluded that the models of the effective thermal conductivities can be unified as $\frac{k_{\text{eff}}}{k_b} = \frac{1}{1 + \alpha Kn}$ in which the parameter α reflects the size effects under different conditions and has been used in [Eq. \(9\)](#). As [Figure 5](#) shows, since the size effect on the effective thermal conductivities changes with r_{12} for a fixed Kn , the value of α should be modified to reflect the boundary

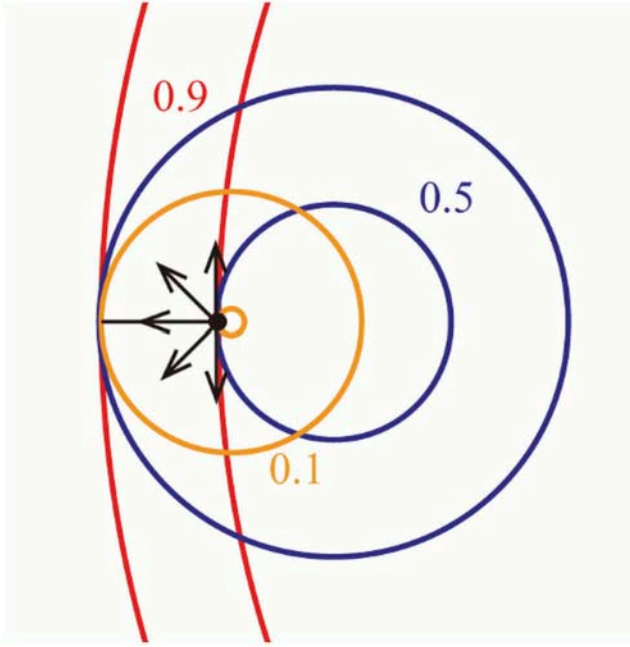


Figure 6. The schematic diagram of different r_{12} for a same L . (Only a part of the boundaries for $r_{12} = 0.9$ is shown).

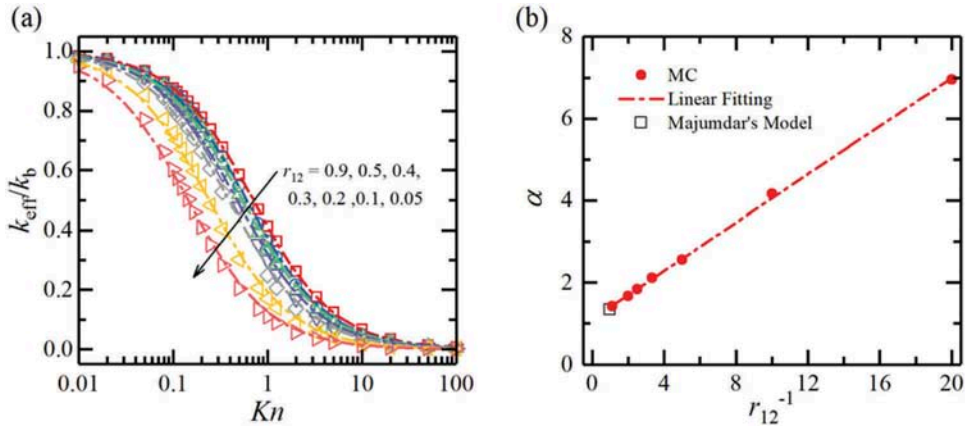


Figure 7. (a) The effective thermal conductivities varying with Kn . The dash-dotted lines are the fitting results of the phonon MC simulations (symbols) by $\frac{k_{\text{eff}}}{k_b} = \frac{1}{1 + \alpha Kn}$. (b) The dependence of α on $1/r_{12}$. Majumdar's result [23] for 1D systems is also depicted.

shape relation in radial heat conduction. The fitted results are shown in Figure 7 (a), where the fairly good agreements with the phonon MC simulations validate its correctness. More importantly, the fitted values of α are linearly related to $1/r_{12}$, as shown in Figure 7 (b). Back to Figure 6, the area of the outer boundary that can be directly 'seen' by the inner boundary of a unit length equals $1/r_{12}$, with which the ballistic effect definitely increases as there will be more phonons being absorbed by the outer boundary without phonon-phonon scattering. As a result, the size effect will be stronger with increasing $1/r_{12}$ though Kn is the same, thus resulting in a larger value of α . The linear fitting in Figure 7 (b) gives $\alpha = 1.11 + 0.29/r_{12}$, which compare favorably with Majumdar's work at $r_{12} = 1$. By using the expression of α , the boundary confined MFP which reflects the intensity of phonon-boundary scattering [29] can be calculated as $l_{\text{bdy}} = L/\alpha$. For $Kn = 0.01$, l_{bdy} is about 25 times the value of l_0 even for $r_{12} = 0.1$,

demonstrating that phonon-phonon scattering is much stronger than phonon-boundary scattering and validating the use of the diffusive approximation quantitatively. Besides, the heat flux at any point within the system can be calculated as $q^*(r) = \frac{4r_2(1-r_{12})}{3 \ln(1/r_{12})(\alpha+1/Kn)} \frac{1}{r}$, from which Eq. (9) is derived to establish the model for boundary temperature jumps.

The effective thermal conductivity is based on the temperature difference and heat flow of the whole system. Except for the total heat flow, the temperature profiles can be employed to define the local thermal conductivity. Instead of Eq. (11), the relation of the local heat flux and local temperature gradient could be assumed to be proportional [22], and the corresponding coefficient is termed as the local thermal conductivity, namely

$$k_{\text{local}}(r) = |q(r) / \nabla T(r)| \quad (12)$$

The subscript ‘local’ means it is a local parameter extracted from the temperature profiles. The statistical error in phonon MC causes the direct calculation of the temperature gradients challenging. As a substitute, the theoretical predictions by Eq. (8) are adopted and the calculated results are shown in Figure 8. It is illustrative that except for the near bulk systems at $Kn = 0.01$, the local thermal conductivity increases distinctly in the heat flow direction. In 1D heat conduction, the heat flux and temperature gradient are constants within the system, making k_{local} be uniform. Consequently, the use of the boundary temperature jump and effective thermal conductivity successfully characterize the phonon transport. However, in radial heat conduction, when ballistic transport cannot be ignored, the corresponding non-linear temperature profiles in Figure 2 leads to a varied $\partial T / \partial \ln r$, and $k_{\text{local}}(r) = \frac{Q}{|dT/d \ln r|}$ is not a constant along the radius direction. In addition, the values of $|dT/d \ln r|$ decrease with r in ballistic regime, thus $k_{\text{local}}(r)$ will increase as Figure 8 demonstrates. Therefore, if a Fourier type equation like Eq. (12) is used to calculate the temperature profile, a varied $k_{\text{local}}(r)$ is needed besides the effective thermal conductivity and boundary temperature jump.

Yang et al. [33] have found the increased local thermal conductivities along the radius direction in nanoscale graphene disks by MD simulations. They asserted that it is caused by the fact that

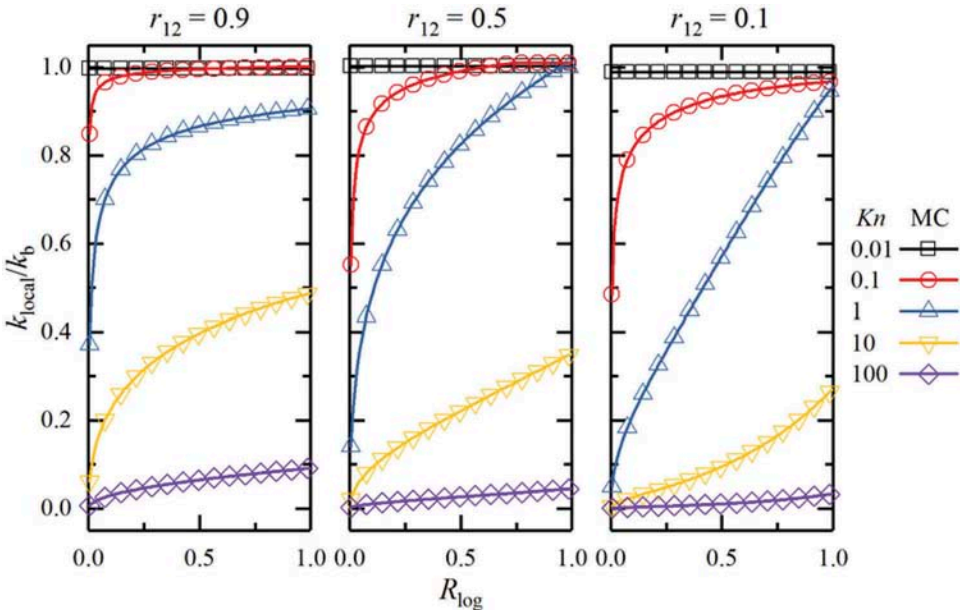


Figure 8. The local thermal conductivities varying in the radius direction. The temperature gradients are calculated by the results of Eq. (8).

nanoscale graphene disks are naturally functionally graded materials. As a contrast, our studies have demonstrated that the ballistic transport in radial heat conduction contributes to the graded local thermal conductivity at nanoscale. In fact, heat conduction has been widely accepted as a non-local process in nanoscale, so the use of a local parameter to describe the thermal transport will lead to some novel phenomena.

Conclusions

In the present work, we study the radial ballistic-diffusive heat conduction at the nanoscale by phonon tracing MC method and theoretical analyses based on phonon BTE. The radial phonon transport is found to be determined by both the Knudsen number and the radius ratio of the boundaries, where the Knudsen number is defined as the ratio of phonon MFP to the difference of the boundary radius.

The temperature distribution within the system is supposed to be linearly dependent on the logarithm coordinate by Fourier's law, but ballistic transport causes it to vary non-linearly and such non-linearity increases with increasing the Knudsen number or decreasing the radius ratio. In addition, ballistic transport leads to boundary temperature jump as it does in 1D systems, but the jump values are not the same at the two boundaries, which is related to the varied temperature gradient along the heat flow direction in radial heat conduction. The differences will be larger as the Knudsen number increases or the radius ratio decreases. Furthermore, based on the idea that Fourier's law and the Casimir limit can be considered as the two bounds of phonon transport, models for the temperature profile and boundary temperature jump has been established by interpolation of the local phonon energy between the limit solutions, which do a good job of matching the results of phonon MC simulations.

To better understand the new-found effect of the radius ratio on phonon transport, the simulated effective thermal conductivities under different radius ratios are fitted by $\frac{k_{\text{eff}}}{k_b} = \frac{1}{1 + \alpha Kn}$ to get $\alpha = 1.11 + 0.29/r_{12}$. Thus, a reduced r_{12} results in stronger size effect of the effective thermal conductivity, even Kn is fixed. Moreover, the local thermal conductivity calculated by local heat flux and local temperature gradient is found to be nonuniform within the system and will increase with the radial coordinate r , which can be interpreted as the outcome of using a local parameter to describe the nonlocal ballistic-diffusive transport.

Considering the nonlinearity of the temperature profile, the difference of the inner and outer boundary temperature jumps and the deviation of the effective thermal conductivity from the bulk value are all going to be more significant as r_{12} decreases, we conclude that besides increasing Kn , decreasing r_{12} will also increase the intensity of ballistic transport compared to the diffusive transport. Such phenomenon is related to the 2D character of radial heat conduction which is affected by both the system size and shape. Our work has highlighted the phonon-boundary scattering and ballistic effect in nanoscale radial heat conduction and could provide a more in-depth understanding as well as some analytical models for the thermal transport in nanofilms, graphene sheets, and encapsulated nanowires.

Funding

This work is financially supported by National Natural Science Foundation of China [No. 51676108], and Science Fund for Creative Research Groups [No. 51621062].

References

- [1] M. Pedram and S. Nazarian, "Thermal modeling, analysis, and management in VLSI circuits: principles and methods," *P. IEEE*, vol. 94, pp. 1487–1501, 2006. DOI:10.1109/JPROC.2006.879797.
- [2] E. Pop, "Energy dissipation and transport in nanoscale devices," *Nano Res.*, no. 3, pp. 147–169, 2010. DOI:10.1007/s12274-010-1019-z.

- [3] S. Reda, "Thermal and power characterization of real computing devices," *IEEE J. EM. SEL. TOP. C.*, vol. 1, pp. 76–87, 2011. DOI:10.1109/JETCAS.2011.2158275.
- [4] S. G. Volz and G. Chen, "Molecular dynamics simulation of thermal conductivity of silicon nanowires," *Appl. Phys. Lett.*, vol. 75, pp. 2056–2058, 1999. DOI:10.1063/1.124914.
- [5] G. Chen, "Ballistic-diffusive heat-conduction equations," *Phys. Rev. Lett.*, vol. 86, pp. 2297–2300, 2001. DOI:10.1103/PhysRevLett.86.2297.
- [6] J. E. Turney, A. J. H. Mcgaughey, and C. H. Amon, "In-plane phonon transport in thin films," *J. Appl. Phys.*, vol. 107, pp. 024317, 2010. DOI:10.1063/1.3296394.
- [7] G. Chen, "Thermal conductivity and ballistic-phonon transport in the cross-plane direction of superlattices," *Phys. Rev. B.*, vol. 57, pp. 14958–14973, 1998. DOI:10.1103/PhysRevB.57.14958.
- [8] A. Sellitto, V. A. Cimmelli, and D. Jou, *Mesoscopic Theories of Heat Transport in Nanosystems*, Cham, Switzerland: Springer International Publishing, 2016.
- [9] E. Pop, S. Sinha, and K. E. Goodson, "Heat generation and transport in nanometer-scale transistors," *P. Ieee.*, vol. 94, pp. 1587–1601, 2006. DOI:10.1109/JPROC.2006.879794.
- [10] S. Ghosh *et al.*, "Dimensional crossover of thermal transport in few-layer graphene," *Nat. Mater.*, vol. 9, pp. 555–558, 2010. DOI: 10.1038/nmat2753.
- [11] R. Mehta, S. Chugh, and Z. Chen, "Enhanced electrical and thermal conduction in graphene-encapsulated copper nanowires," *Nano Lett.*, vol. 15, pp. 2024–2030, 2015. DOI:10.1021/nl504889t.
- [12] D. G. Cahill, "Analysis of heat flow in layered structures for time-domain thermoreflectance," *Rev. Sci. Instrum.*, vol. 75, pp. 5119–5122, 2004. DOI:10.1063/1.1819431.
- [13] M. Asheghi, Y. K. Leung, S. S. Wong, and K. E. Goodson, "Phonon-boundary scattering in thin silicon layers," *Appl. Phys. Lett.*, vol. 71, pp. 1798–1800, 1997. DOI:10.1063/1.119402.
- [14] W. Liu and M. Asheghi, "Phonon-boundary scattering in ultrathin single-crystal silicon layers," *Appl. Phys. Lett.*, vol. 84, pp. 3819–3821, 2004. DOI:10.1063/1.1741039.
- [15] W. Liu, K. Etessam-Yazdani, R. Hussin, and M. Asheghi, "Modeling and data for thermal conductivity of ultrathin single-crystal SOI layers at high temperature," *IEEE T. Electron Dev.*, vol. 53, pp. 1868–1876, 2006. DOI:10.1109/TED.2006.877874.
- [16] A. A. Maznev *et al.*, "Direct measurement of room-temperature nondiffusive thermal transport over micron distances in a silicon membrane," *Phys. Rev. Lett.*, vol. 110, pp. 025901, 2013. DOI: 10.1103/PhysRevLett.110.025901.
- [17] H. B. G. Casimir, "Note on the conduction of heat in crystals," *Physica.*, vol. 5, pp. 495–500, 1938. DOI:10.1016/S0031-8914(38)80162-2.
- [18] B. W. Li and J. Wang, "Anomalous heat conduction and anomalous diffusion in one-dimensional systems," *Phys. Rev. Lett.*, vol. 91, pp. 044301, 2003. DOI:10.1103/PhysRevLett.91.044301.
- [19] F. X. Alvarez and D. Jou, "Memory and nonlocal effects in heat transport: from diffusive to ballistic regimes," *Appl. Phys. Lett.*, vol. 90, pp. 083109, 2007. DOI:10.1063/1.2645110.
- [20] F. X. Alvarez, D. Jou, and A. Sellitto, "Phonon hydrodynamics and phonon-boundary scattering in nanosystems," *J. Appl. Phys.*, vol. 105, pp. 014317, 2009. DOI:10.1063/1.3056136.
- [21] C. Jeong, S. Datta, and M. Lundstrom, "Thermal conductivity of bulk and thin-film silicon: a Landauer approach," *J. Appl. Phys.*, vol. 111, pp. 093708, 2012. DOI:10.1063/1.4710993.
- [22] K. Aoki and D. Kusnezov, "Fermi-Pasta-Ulam beta model: boundary jumps, Fourier's law, and scaling," *Phys. Rev. Lett.*, vol. 86, pp. 4029–4032, 2001. DOI:10.1103/PhysRevLett.86.4029.
- [23] A. Majumdar, "Microscale heat conduction in dielectric thin films," *J. Heat. Trans.*, vol. 115, pp. 7–16, 1993. DOI:10.1115/1.2910673.
- [24] Y. C. Hua and B. Y. Cao, "Phonon ballistic-diffusive heat conduction in silicon nanofilms by Monte Carlo simulations," *Int. J. Heat Mass Tran.*, vol. 78, pp. 755–759, 2014. DOI:10.1016/j.ijheatmasstransfer.2014.07.037.
- [25] J. Maassen and M. Lundstrom, "Steady-state heat transport: ballistic-to-diffusive with Fourier's law," *J. Appl. Phys.*, vol. 117, pp. 011305, 2015. DOI:10.1063/1.4905590.
- [26] S. L. Sobolev, "Discrete space-time model for heat conduction: application to size- dependent thermal conductivity in nano-films," *Int. J. Heat Mass Tran.*, vol. 108, pp. 933–939, 2017. DOI:10.1016/j.ijheatmasstransfer.2016.12.051.
- [27] S. Lepri, R. Livi, and A. Politi, "Thermal conduction in classical low-dimensional lattices," *Phys Rep.*, vol. 377, pp. 1–80, 2003. DOI:10.1016/S0370-1573(02)00558-6.
- [28] J. Chen, G. Zhang, and B. W. Li, "A universal gauge for thermal conductivity of silicon nanowires with different cross sectional geometries," *J. Chem. Phys.*, vol. 135, pp. 204705, 2011. DOI:10.1063/1.3663386.
- [29] Y. C. Hua and B. Y. Cao, "Ballistic-diffusive heat conduction in multiply-constrained nanostructures," *Int. J. Therm. Sci.*, vol. 101, pp. 126–132, 2016. DOI:10.1016/j.ijthermalsci.2015.10.037.
- [30] Y. C. Hua and B. Y. Cao, "Anisotropic heat conduction in two-dimensional periodic silicon nanoporous films," *J. Phys. Chem. C.*, vol. 121, pp. 5293–5301, 2017. DOI:10.1021/acs.jpcc.6b11855.
- [31] A. Sellitto, D. Jou, and J. Bafaluy, "Non-local effects in radial heat transport in silicon thin layers and graphene sheets," *P. Roy. Soc. A-Math. Phys.*, vol. 468, pp. 1217–1229, 2012. DOI:10.1098/rspa.2011.0584.
- [32] A. Sellitto and V. A. Cimmelli, "Flux limiters in radial heat transport in silicon nanolayers," *J. Heat. Trans.*, vol. 136, pp. 071301, 2014. DOI:10.1115/1.4027183.

- [33] N. Yang, S. Hu, D. Ma, T. Lu, and B. Li, “Nanoscale graphene disk: a natural functionally graded material—how is Fourier’s law violated along radius direction of 2D disk,” *Sci. Rep.-UK*, vol. 5, pp. 14878, 2015. DOI:10.1038/srep14878.
- [34] R. B. Wilson and D. G. Cahill, “Anisotropic failure of Fourier theory in time-domain thermoreflectance experiments,” *Nat. Commun.*, vol. 5, pp. 5075, 2014. DOI:10.1038/ncomms6075.
- [35] M. F. Modest, *Radiative Heat Transfer*, 2nd ed., Cambridge: Academic Press, 2003.
- [36] Y. C. Hua and B. Y. Cao, “Slip boundary conditions in ballistic-diffusive heat transport in nanostructures,” *Nanoscale Microsc. Therm.* no. 3, pp. 159–176, 2017. DOI:10.1080/15567265.2017.1344752.
- [37] J. P. M. Péraud and N. G. Hadjiconstantinou, “An alternative approach to efficient simulation of micro/nanoscale phonon transport,” *Appl. Phys. Lett.*, vol. 101, pp. 153114, 2012. DOI:10.1063/1.4757607.
- [38] Y. Hu, L. Zeng, A. J. Minnich, M. S. Dresselhaus, and G. Chen, “Spectral mapping of thermal conductivity through nanoscale ballistic transport,” *Nat. Nanotechnol.*, vol. 10, pp. 701–706, 2015. DOI:10.1038/NNANO.2015.109.
- [39] R. Kt *et al.*, “Broadband phonon mean free path contributions to thermal conductivity measured using frequency domain thermoreflectance,” *Nat. Commun.*, vol. 4, pp. 1640–1646, 2013. DOI: 10.1038/ncomms2630.
- [40] T. Feng *et al.*, “Spectral analysis of nonequilibrium molecular dynamics: spectral phonon temperature and local nonequilibrium in thin films and across interfaces,” *Phys. Rev. B.*, vol. 95, pp. 195202, 2017. DOI: 10.1103/PhysRevB.95.195202.
- [41] K. Kukita and Y. Kamakura, “Monte Carlo simulation of phonon transport in silicon including a realistic dispersion relation,” *J. Appl. Phys.*, vol. 114, pp. 154312, 2013. DOI:10.1063/1.4826367.
- [42] Y. C. Hua and B. Y. Cao, “Cross-plane heat conduction in nanoporous silicon thin films by phonon Boltzmann transport equation and Monte Carlo simulations,” *Appl. Therm. Eng.*, vol. 111, pp. 1401–1408, 2016. DOI:10.1016/j.applthermaleng.2016.05.157.
- [43] Y. C. Hua and B. Y. Cao, “Interface-based two-way tuning of the in-plane thermal transport in nanofilms,” *J. Appl. Phys.*, vol. 123, pp. 114304, 2018. DOI:10.1063/1.5013657.
- [44] F. Yang and C. Dames, “Mean free path spectra as a tool to understand thermal conductivity in bulk and nanostructures,” *Phys. Rev. B.*, vol. 87, pp. 035437, 2013. DOI:10.1103/PhysRevB.87.035437.
- [45] Y. S. Ju and K. E. Goodson, “Phonon scattering in silicon films with thickness of order 100 nm,” *Appl. Phys. Lett.*, vol. 74, pp. 3005–3007, 1999. DOI:10.1063/1.123994.
- [46] M. Jeng, R. Yang, D. Song, and G. Chen, “Modeling the thermal conductivity and phonon transport in nanoparticle composites using Monte Carlo simulation,” *J. Heat. Trans.*, vol. 130, pp. 042410, 2008. DOI:10.1115/1.2818765.
- [47] H. L. Li, Y. C. Hua, and B. Y. Cao, “A hybrid phonon Monte Carlo-diffusion method for ballistic-diffusive heat conduction in nano- and micro- structures,” *Int. J. Heat Mass Tran.*, vol. 127, pp. 1014–1022, 2018. DOI:10.1016/j.ijheatmasstransfer.2018.06.080.
- [48] D. B. Olfe, “Application of a modified differential approximation to radiative transfer in a gray medium between concentric spheres and cylinders,” *J. Quant. Spectrosc. Ra.*, vol. 8, pp. 899–907, 1968. DOI:10.1016/0022-4073(68)90094-0.
- [49] J. R. Howell, M. P. Mengüç, and R. Siegel, *Thermal Radiation Heat Transfer*, 6th ed. Florida: CRC Press, 2015.
- [50] G. Chen, “Nonlocal and nonequilibrium heat conduction in the vicinity of nanoparticles,” *J. Heat. Trans.*, vol. 118, pp. 539–545, 1996. DOI:10.1115/1.2822665.
- [51] Y. C. Hua and B. Y. Cao, “The effective thermal conductivity of ballistic-diffusive heat conduction in nanostructures with internal heat source,” *Int. J. Heat Mass Tran.*, vol. 92, pp. 995–1003, 2016. DOI:10.1016/j.ijheatmasstransfer.2015.09.068.